Negative refraction and photonic-crystal optics in a cold gas

Marina Litinskaya and Evgeny A. Shapiro
Department of Chemistry, University of British Columbia, Vancouver V6T 1Z1, Canada
(Received 14 June 2014; revised manuscript received 3 January 2015; published 3 March 2015)

We describe propagation of light in a gas with periodic density modulation, demonstrating photonic-crystal-like refraction with negative refraction angles. We address the role of poorly defined boundaries and damping and derive an optical analog of the quantum adiabatic theorem. For Cs atoms in an optical lattice, we show that relying on semiadiabatic propagation one can excite and spatially split positively and negatively refracting modes at experimentally available gas densities.

DOI: 10.1103/PhysRevA.91.033802 PACS number(s): 42.70.Qs, 37.10.Jk, 78.20.Ci

I. INTRODUCTION

A wave is negatively refracted at an interface of two media if its group velocity component along the interface changes its sign [1], as shown in Fig. 1(a). Fascinating optical effects based on negative refraction include invisibility [2], near-field focusing with planar devices [3], seeing around a corner [4], and superprism [5].

This work is aimed at achieving negative refraction in a gas. Using laser fields instead of nanofabrication for preparing the sample will enable dynamical real-time control at a distance in the optical frequency domain [6,7]. New applications such as nonlinear spectroscopy with backward propagating signal [8] may become available.

As is known, photonic crystal metamaterials offer a route to negative refraction [9]. Both negatively and positively refracted modes appear due to periodic modulation of the dielectric constant, see Fig. 1(b). We shall call them "N" and "P"modes, respectively, implying both the negative-like refraction in 1D photonic crystals and true negative refraction in 2D photonic crystals, where Snell's law with a negative refractive index is in effect [10]. Below we theoretically demonstrate the possibility of negative-like refraction in a cold gas trapped in an optical lattice. Its prerequisite, photonic band gap, is routinely observed in such systems [11]. We study negative refraction in the proof of principle case of 1D periodicity; implementation in 2D and 3D is straightforward. The scheme offers low gas densities, simple design, and a large frequency window of negative refraction.

In a gas, the intuition coming from the photonic crystal optics meets two challenges. First, due to low densities, a significant modulation of the dielectric constant is only possible in a narrow vicinity of a resonance, where absorption is high (here the term "absorption" and the damping associated with it refer to the elastic scattering of light into other electromagnetic modes of the environment). This resonant absorption can be overcome using schemes based on electromagnetically induced transparency (EIT) [12]. Here we study another route: For a thermal gas trapped in a 1D optical lattice, we consider relatively large detuning from the resonance so both absorption and modulation of the refractive index are moderate. The negative-like refraction emerges due to periodicity of the lattice potential. The required gas density turns out to be experimentally achievable 10^{13} cm^{-3} [13], three to five orders of magnitude lower than in the earlier proposals on negative refraction in a gas [6,7]. As discussed below, the advantage comes both from not relying on the weak magnetic response of the gas and from the N mode being immune to resonant absorption.

The second challenge, common for all gaseous samples, is due to poorly defined boundaries in a gas cloud. As discussed below, if light penetrates the cloud adiabatically, then only the P mode is excited and negative refraction is never achieved. It turns out that this challenge can be overcome. We derive an analog of the quantum adiabatic theorem for coupled propagation of N and P modes and study the dynamics of energy transfer between them. We show that with experimentally achievable conditions one can realize propagation possessing both adiabatic and nonadiabatic features, thus providing transfer into the N mode and simultaneously avoiding unwanted reflection at boundaries.

II. WAVES IN RESONANT PERIODIC ARRAYS

A 1D photonic crystal with a period a comparable with a half of the light wavelength λ [Fig. 1(b)] acts as a volume diffraction grating and supports P- and N-diffracted modes [10,14]. We model an infinite (so the boundary is irrelevant) grating as a periodic set of δ-like perturbations in the dielectric constant:

$$\varepsilon(z;\omega) = 1 + \varepsilon_c d \sum_n \delta(z - na) = 1 + \frac{d}{a}\varepsilon_c \sum_n e^{inzG}, \quad (1)$$

where $G = 2\pi/a$ and ε_c is the dielectric contrast between the layers of the grating and vacuum. The use of the δ-function limit of the Kronig-Penney model for the atomic density distribution in Eq. (1) is substantiated by the parameters of nowadays experiments. For a typical optical lattice trapping frequency about 100 kHz, the thickness d of a single atomic layer, estimated as the size of ground-state wave function in a lattice cite, is about 30 nm, whereas the interlayer distance a is 532 nm (the lattice light wavelength $\lambda = 1024$ nm). The position spread of the atoms reduces the strength of the Bragg signal by the Debye-Waller factor $\beta = \exp[-2\pi^2 d^2/a^2]$; values of β as low as 0.2 already lead to well-defined Bragg pattern (see Birkl *et al.* in Ref. [11]). For our parameters, $\beta = 0.94 \approx 1$. This implies that light scattering is barely affected by the deviation of the atomic density distribution from a set of δ functions.

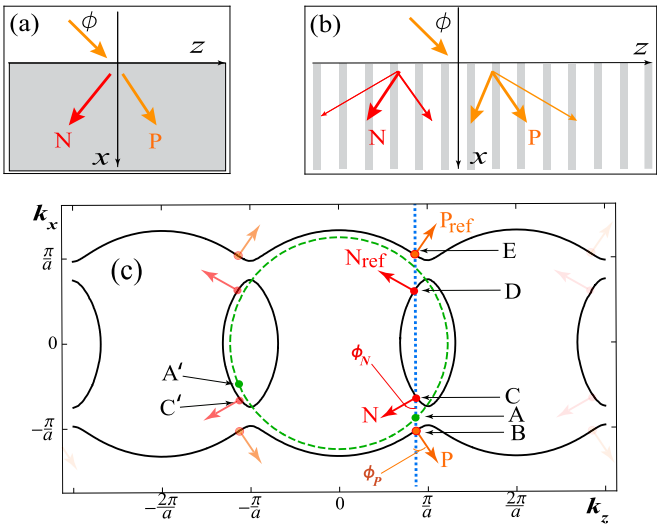

FIG. 1. (Color online) (a) Negative (red) and positive (gold) refraction at an interface. (b) Negative and positive Floquet-Bloch modes in a 1D photonic crystal. (c) Solid black line: EFS in a 1D photonic crystal. Green dashed circle: EFS for light in vacuum. Red and gold arrows show the propagation directions of the N and P modes. Points A, A′ denote the incident and outgoing light beams in free space, as discussed in the text. Points B, C, D, and E denote the P, N, $N_{\rm ref}$ and $P_{\rm ref}$ modes.

The Maxwell wave equation in a periodic in z and homogeneous in x medium can be written as

$$\hat{M}E = -\partial^2 E/\partial x^2, \tag{2}$$

where

$$\hat{M} = \partial^2/\partial z^2 + \varepsilon(z,\omega)\omega^2/c^2. \tag{3}$$

Due to periodicity along z, its solutions for TE-polarized waves, $\mathbf{E} = (0,E,0)$ and $\mathbf{H} = (H_x,0,H_z)$, are Floquet-Bloch modes [14] consisting of partial waves (marked by index m) of the form

$$E(x,z;t) = \sum_m C_m \exp\{i[k_x x + (k_z + mG)z - \omega t]\}. \tag{4}$$

Substituting (1) into (2) and (3), after simple algebra we find the amplitudes C_m,

$$C_m = \frac{\varepsilon_c \omega^2 \left(\sum_l C_l\right)}{c^2\left[k_x^2 + (k_z + mG)^2\right] - \omega^2}. \tag{5}$$

The dispersion equation for ω, k_x, and k_z,

$$\cos ak_z = \cos ak_z^{(\rm vac)} - \frac{d}{a}\frac{\varepsilon_c}{2}\left(\frac{\omega a}{c}\right)^2 \frac{\sin ak_z^{(\rm vac)}}{ak_z^{(\rm vac)}}, \tag{6}$$

where $k_z^{(\rm vac)} = \sqrt{\frac{\omega^2}{c^2} - k_x^2}$, is obtained by summing (5) over m, canceling $\sum_m C_m$ and $\sum_l C_l$ and calculating the remaining sum over m in the right-hand side [15]. Floquet-Bloch modes of the form (4) and (5) are sketched in Fig. 1(b). The arrows show phase velocity directions. Amplitude of m-th partial wave is determined by the corresponding denominator in the right-hand side of Eq. (5), i.e., by how close to ω^2/c^2 each $k_x^2 + (k_z + mG)^2$ is, and is shown schematically by the arrow thickness. The group velocity is the same for all partial waves in a mode.

The number of different Floquet-Bloch modes with the same value of k_z and their propagation directions can be deduced from the equifrequency surface (EFS) for Eq. (6) in the k_x,k_z plane [10,14,16]. Figure 1(c) shows an example EFS for the frequency $\omega = 1.25\pi c/a$, strong modulation of ε, and negligible absorption. The periodicity results in the EFS diagram with the property $\omega(k_x,k_z) = \omega(k_x,k_z + mG)$ for all m: Instead of a single circle $k_x^2 + k_z^2 = \omega^2/c^2$ (green dashed circle in the figure), EFS consists of a series of circles corresponding to different partial waves. In addition, at $k_z = G/2 + mG$ there are Bragg gaps, which change the topology of the EFS: Instead of intersecting circles corresponding to the bare photon dispersion repeated along k_z, there is a series of smaller inner ellipses embraced by merging outer parts of the circles. Each Floquet-Bloch mode of the photonic crystal is characterized by a specific value of k_x, and a set of $k_z = k_{z0} + mG$, $m = 0, \pm 1, \pm 2, \ldots$. In Fig. 1(c) they are represented by points on the EFS. For instance, points C and C′ belong to the same mode: C marks its partial wave with $m = 0$, C′ marks $m = -1$.

Consider a light beam incident from $x = -\infty$ at an angle ϕ as shown in Fig. 1(b). This beam is represented by point A on the green dashed circle $\sqrt{k_{x0}^2 + k_{z0}^2} = \omega/c$ in Fig. 1(c). At the boundary, it can couple to all the Floquet-Bloch modes with the same value of $k_{z0} = (\omega/c)\sin\phi$. Intersections of the line $k_z = k_{z0}$ (dotted blue line) with the EFS determine the k_x values of the eigenmodes coupled to the probe. Normals to the EFS [depicted by arrows in Fig. 1(c)] determine the group velocity directions of these modes [10,14,16]. The figure shows that for k_{z0} close to π/a there are two normal modes with positive x component of the group velocity: an N mode (with $k_x \equiv k_N$, point C) and a P mode (with $k_x \equiv k_P$, point B). Note that the N mode exhibits negative-like refraction. Points D and E with the same k_{z0} and $k_x = -k_{N,P}$ correspond to two reflected waves, denoted as $N_{\rm ref}$ and $P_{\rm ref}$.

The size of the gap at $k_z = \pi/a$ is determined by the value of ε_c in Eq. (1). In conventional photonic crystals, the contrast ε_c comes from remote resonances (background dielectric constant). In a gas with the mean density ρ, substantial contrast appears only near an atomic resonance, ω_T [17]:

$$\frac{d}{a}\varepsilon_c \to \varepsilon_{\rm res}(\omega) = \frac{8\pi\omega_T\mu^2\rho}{\omega_T^2 - \omega^2 - 2i\omega_T\gamma}, \tag{7}$$

where μ is the dipole transition matrix element and γ accounts for losses. Below we imply that the periodic structure shown on Fig. 1(b) depicts atoms in a 1D optical lattice. The calculations are done for the D2 line of Cs ($\mu = 4.48$ a.u., $\omega_T = 11732$ cm^{-1}) in a lattice with $a = 532$ nm. Both the Doppler and collisional widths at $T \ll 1$ K are negligible compared to the radiative broadening $\gamma \simeq 33$ MHz [18]. At large detunings considered below, the EFS of Fig. 1(c) remains qualitatively valid; at small detunings it washes out due to absorption.

III. DYNAMICS OF COUPLED MODES AT THE BOUNDARY

Inside the gas cloud, the dielectric contrast is a function of the penetration depth: $\varepsilon_{\rm res}(x,\omega) = \alpha(x)\varepsilon_{\rm res}(\omega)$. Here $\alpha(x)$ is the density profile characterized by two scales: the total

length of the cloud, L, and the length of the entrance and exit zones, L_*. In these zones $\alpha(x)$ varies between 0 (vacuum) and 1 (peak density). Each value of x can be assigned its own EFS diagram. As x grows, EFS gradually transforms from a single circle $\sqrt{k_x^2+k_z^2}=\omega/c$ to a periodic structure similar to that shown in Fig. 1(c) by the thick black line. The free-space mode shown by point A adiabatically connects upon such gradual transformation with the P mode characterized by the same value of k_z (point B). Therefore, if the gas density at the boundary changes slowly, then transfer of energy from the P mode both to the (wanted) N mode (point C) and (unwanted) reflected modes (points D and E) is suppressed.

Let us consider the dynamics of coupled modes in a lossy gas with a poorly defined gas-vacuum interface. We introduce a "local basis" for light eigenmodes, assuming that $\alpha(x)$ is a relatively slow function. Namely, we assume that at each x the expressions (5) and (6) hold with $\alpha(x)\varepsilon_{\rm res}(\omega)$ replacing ε_c. Now $\hat{M}\to\hat{M}(x)$, and for fixed ω and k_z, Eq. (5) defines the x-dependent amplitudes $C_m(x)$, and Eq. (6) defines the x component of the total wave vector, $k_x(x)$. For ω and k_z of interest, both the N and P modes can propagate, and we write the total electric field in the form:

$$E=c_N(x)\,|N(x)\rangle e^{i\int_0^x \mathfrak{K}_N(x_1)\,dx_1}+c_P(x)\,|P(x)\rangle e^{i\int_0^x \mathfrak{K}_P(x_1)\,dx_1}, \tag{8}$$

where $\mathfrak{K}_{N,P}=\mathrm{Re}[k_{N,P}]$ are the real parts of $k_x=k_{N,P}$ found from Eq. (6). $|N(x)\rangle$ and $|P(x)\rangle$ stand for the N and P eigenmodes of the type (4) calculated in the local basis:

$$|Y(x)\rangle=\sum_m Y_m(x)\,\exp[i((k_z+mG)z-\omega t)]. \tag{9}$$

Here $Y=N,P$, and $Y_m=N_m,P_m$ are the partial wave amplitudes in each of the eigenmodes. Coupling to the reflected modes is neglected on the basis of higher adiabaticity, as explained in Sec. IV. The damping is included into the mode amplitudes $c_N(x)$ and $c_P(x)$ through $\mathrm{Im}[k_{N,P}(x)]$. As compared to damping-free propagation, the damping leads to decline of the amplitudes as x grows. Each eigenmode is normalized as $\langle Y|Y\rangle=4\pi\omega/(c^2\mathfrak{K}_Y)$ [19–21]. This normalization corresponds to a unit energy flow across the plane $x=$ const for zero damping.

To find the amplitudes $c_P(x)$ and $c_N(x)$, we substitute Eq. (8) into the wave equation (2), (3) with $\varepsilon(x,z,\omega)=\alpha(x)\varepsilon(z,\omega)$ and $\hat{M}=\hat{M}(x)$. Using Eq. (5) for the amplitudes of the partial waves, one can check that at a given x,

$$\begin{aligned}\hat{M}(x)|N(x)\rangle&=k_N^2(x)|N(x)\rangle,\\ \hat{M}(x)|P(x)\rangle&=k_P^2(x)|P(x)\rangle.\end{aligned} \tag{10}$$

We apply the slow envelope approximation [17], assuming that x derivatives of all involved quantities are small compared to $k_{P,N}$. Making use of Eq. (10), we find that the wave equation is satisfied if (prime denotes x derivative)

$$\begin{aligned}&\big[2\mathfrak{K}_N c_N'|N\rangle+2\mathfrak{K}_N c_N|N'\rangle\\ &\quad+\big(\mathfrak{K}_N'+i\big(\mathfrak{K}_N^2-k_N^2\big)\big)c_N|N\rangle\big]e^{i\int_0^x dx_1\mathfrak{K}_N(x_1)}\\ &\quad+\big[2\mathfrak{K}_P c_P'|P\rangle+2\mathfrak{K}_P c_P|P'\rangle\\ &\quad+\big(\mathfrak{K}_P'+i\big(\mathfrak{K}_P^2-k_P^2\big)\big)c_P|P\rangle\big]e^{i\int_0^x dx_1\mathfrak{K}_P(x_1)}=0.\end{aligned} \tag{11}$$

We consecutively multiply (11) by $\langle N|$ and $\langle P|$. The resulting equations can be simplified by noticing that ($Y=N,P$)

$$\begin{aligned}\mathrm{Re}[\langle Y|Y'\rangle]&=-\frac{2\pi\omega\mathfrak{K}_Y'}{c^2\mathfrak{K}_Y^2},\\ \langle N|P'\rangle&=\langle P'|N\rangle^*=-\langle P|N'\rangle^*.\end{aligned} \tag{12}$$

These equalities are obtained by differentiating over x the normalization condition $\langle Y|Y\rangle=4\pi\omega/(c^2\mathfrak{K}_Y)$ and the orthogonality condition $\langle P|N\rangle=0$. Now from Eq. (11) follow the coupled equations for $c_N(x)$ and $c_P(x)$:

$$\begin{aligned}c_N'&=\xi^*\mathfrak{K}_P\,c_P\exp\left[i\int_0^x(\mathfrak{K}_P-\mathfrak{K}_N)dx_1\right]-i\eta_N\mathfrak{K}_N\,c_N\\ c_P'&=-\xi\mathfrak{K}_N\,c_N\exp\left[-i\int_0^x(\mathfrak{K}_P-\mathfrak{K}_N)dx_1\right]-i\eta_P\mathfrak{K}_P\,c_P,\end{aligned} \tag{13}$$

where

$$\begin{aligned}\xi&=\frac{c^2}{4\pi\omega}\langle P|N'\rangle,\\ \eta_Y&=\frac{c^2}{4\pi\omega}\mathrm{Im}[\langle Y|Y'\rangle]+\frac{1}{2}\left(1-\frac{k_Y^2}{\mathfrak{K}_Y^2}\right).\end{aligned} \tag{14}$$

Note that $\mathrm{Im}[\eta_Y\mathfrak{K}_Y]=-\mathrm{Im}[k_Y]$, and the losses due to absorption in Eq. (13) are defined by $\mathrm{Im}[k_Y]$ as expected.

IV. ADIABATICITY CRITERIUM

Equations (13) resemble the equations describing two-state quantum dynamics with the time derivative replaced by the x derivative. To obtain a simple qualitative criterium of adiabaticity for light propagation, we draw an analogy with the quantum adiabatic theorem [22]. Similarly to the quantum two-level dynamics, coupling between the light modes averages out if

$$|\xi\mathfrak{K}_{P,N}|\ll|\mathfrak{K}_P-\mathfrak{K}_N| \tag{15}$$

at all x. We estimate ξ in Eq. (14) for negligible damping, when $\eta_N\approx\eta_P\approx 0$, so $\mathfrak{K}_Y\equiv k_Y$. We differentiate the first of the equations (10) over x, multiply the result by $\langle P|$, and use the complex conjugate of the second of Eqs. (10). Using the orthogonality of $|N(x)\rangle$ and $|P(x)\rangle$ at each x, we find that

$$\langle P|\hat{M}'|N\rangle=\big(k_P^2-k_N^2\big)\langle P|N'\rangle. \tag{16}$$

The left-hand side can be transformed using the definition (3) of the operator $\hat{M}$:

$$\begin{aligned}\langle P|\hat{M}'|N\rangle&=\alpha'\frac{\omega^2}{c^2}\langle P|\varepsilon(\omega,z)|N\rangle\\ &=\alpha'\frac{\omega^2}{c^2}\varepsilon_{\rm res}(\omega)\sum_{nm}P_m^*N_n,\end{aligned} \tag{17}$$

where N_m and P_m are x-dependent mode amplitudes defined in (9). For the density profile $\alpha(x)=\sin^2(\pi x/2L_*)$ used below in the numerical calculations, we replace α' with $\pi/2L_*$ and find:

$$\xi=\frac{\omega\varepsilon_{\rm res(\omega)}}{8vL_*\big(k_P^2-k_N^2\big)}, \tag{18}$$

where $v=1/|\sum_{mn}P_m^*N_n|$ is a constant of the dimension of velocity, ranging from several atomic units in the regions

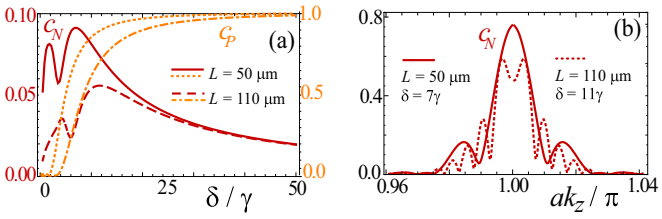

FIG. 2. (Color online) (a) Amplitudes $|c_P(L)|$ (gold, right scale) and $|c_N(L)|$ (red, left scale) in dependence on L and δ with $L_* = 20\ \mu$m. (b) $|c_N(L)|$ at $x = L$ as a function $k_z = \omega/c \sin\phi$ for two sets of parameters.

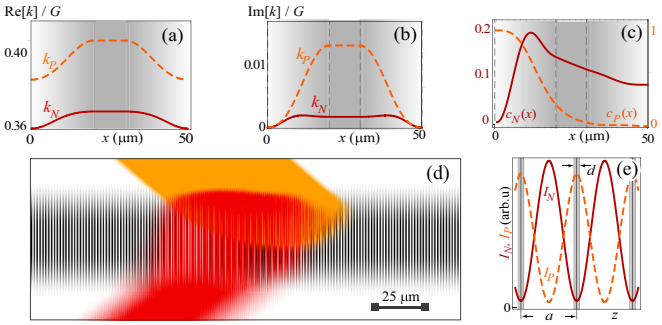

FIG. 3. (Color online) Strong absorption ($\delta = 2\gamma$). Spatial dependence of the real (a) and imaginary (b) parts of k_N and k_P and of c_N and c_P (c). Dashed vertical lines mark the entrance and exit zones. (d) Beam propagation through the cloud. Gold shows the P beam and red the N beam. (e) Intensity profiles of the modes along z at $L = L_*$.

of low gas density and small adiabaticity to about 18 a.u. at $\rho = 10^{13}$ cm^{-3} (the speed of light $c = 137$ a.u.).

The coupling between the modes is only effective in the regions of low adiabaticity, where $k_P \simeq k_N$. Then $k_{P,N}/(k_P + k_N) \simeq 1/2$, and Eq. (15) reduces to the following condition for dynamics to be adiabatic:

$$\Omega_A \equiv L_*(k_P - k_N)^2 \frac{16\,v}{\omega\varepsilon_{\rm res}} \gg 1. \qquad (19)$$

Ω_A is the adiabaticity parameter. The condition $\Omega_A = 1$, which separates regimes of adiabatic and nonadiabatic dynamics, corresponds to L_* ranging from a submicron scale to tens of microns for different angles of incidence. Figure 2 demonstrates the lengths and incidence angles, which result in nonadiabatic coupling between the P and N modes. A discussion of the role of these parameters is in the next section.

Equation (19) shows that the transfer between the modes only takes place if their wave vectors are sufficiently close. The latter observation allowed us to neglect the reflected modes in Eq. (8): At the values of L_* such that the evolution of coupled P and N modes corresponding to points B and C in Fig. 1(c) is barely nonadiabatic, coupling to the reflected modes corresponding to the points D and E can be neglected due to larger $|k_P - k_{P_{\rm ref},N_{\rm ref}}|$. This differs from conventional photonic crystals, where $L_* = 0$ and reflection at the boundary is always present.

V. NUMERICAL RESULTS

For light entering a cloud of Cs atoms in an optical lattice, Eqs. (13) are solved numerically with the boundary conditions $c_N(0) = 0, c_P(0) = 1$. The amplitude $c_N(L)$ at the exit depends on four key parameters. On one hand, $L_*, k_z = (\omega/c)\sin\phi$, and the detuning $\delta = \omega - \omega_T$ determine the adiabaticity parameter Ω_A. On the other hand, δ and L determine losses due to absorption. The smaller the δ, the larger the (wanted) dielectric contrast and (unwanted) absorption.

In Fig. 2(a) we plot the amplitudes at the exit, $|c_N(L)|$, $|c_P(L)|$, as functions of δ for $L = 50$ and 110 μm, with $L_* = 20\ \mu$m, $\rho = 10^{13}$ cm^{-3}, $k_z = 0.98\ \pi/a$, and $\alpha(x) = 1$ inside the cloud and changing according to $\sin^2(\pi x/2L_*)$ law at the boundaries. We have checked numerically that the dependence of the results on the exact profile $\alpha(x)$ is small in comparison with their dependence on the other parameters examined in the paper (angle, detuning, and the entrance region size L_*) as long as $\alpha(x)$ is smooth and changes from 0 to 1 within, approximately, L_*. The $\sin^2$ profile used in this section clearly distinguishes between the boundary zones and that of the peak density, thus making the discussion more transparent.

For $k_z = 0.98\ \pi/a$, the amplitude $c_N(L)$ in Fig. 2 reaches values 0.05–0.1 in the frequency window as large as 20γ, i.e., over 2.5 GHz, slowly declining at larger detunings. For strong absorption ($\delta < 2\gamma$ for our geometry), coupling between the modes is only effective at the entrance: The P mode is completely absorbed at $x \lessapprox L_*$, see the dynamics of $c_{P,N}(x)$ in Fig. 3(c). The N mode survives, experiencing much lower absorption, due to reasons discussed below. In the regime of small absorption ($\delta > 20\gamma$) $c_P(L) \simeq 1$, and $c_{P,N}(L)$ do not depend on L. We observed that at higher densities, starting from $\rho \sim 10^{14}$ cm^{-3}, the energy transfer dynamics strongly resembles that in a Landau-Zener transition [23]. At intermediate absorption, the values $c_P(L)$ and $c_N(L)$ are comparable. Figure 2(b) shows the angular dependence of $|c_N(L)|$ and $|c_P(L)|$ calculated for the same density profiles as in Fig. 2(a). The value $k_z = 0.98\pi/a$, used in the rest of our calculations for illustrative purposes, is at the edge of the window of allowable angles. Closer to the Bragg angle, $|c_N(L)|$ can be as high as 0.8.

Figure 3 illustrates propagation of a Gaussian beam with the central wave vector $k_z = 0.98\ \pi/a$, $\delta = 2\ \gamma$, through a cloud with $L_* = 20\ \mu$m, $L = 50\ \mu$m. The intensities of the two modes in Fig. 3(d) are calculated by expanding the incident beam into plain waves, each with its own k_x,k_z. For each of them we write $E(x,z;t)$ as in Eqs. (5) and (8), and propagate it according to Eqs. (13). Then we combine the waves to retrieve the overall field. The resulting angles of propagation of the P and N beams, ϕ_N and ϕ_P, correspond to the curvature of the EFS at points B and C in Fig. 1(c).

According to Figs. 3(a) and 3(c), transfer between the modes is only efficient for $x \leqslant 10\ \mu$m, where the distance between $\Re_N$ and $\Re_P$ is minimal and dynamics have nonadiabatic features, cf. Eq. (19). The P mode is completely absorbed (rescattered into other modes), while the N mode propagates as a coherent signal with minimal absorption. As the gas density at the exit of the cloud decreases, all the amplitudes

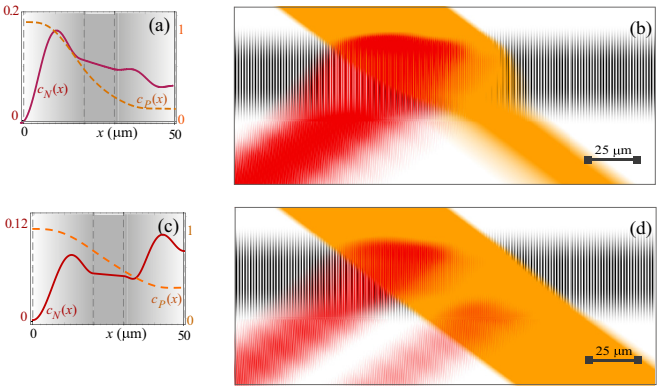

FIG. 4. (Color online) Same as in Figs. 3(c) and 3(d) but for intermediate and weak absorption: $\delta = 3\gamma$ [(a) and (b)] and $\delta = 7\gamma$ [(c) and (d)].

N_m except N_{-1}, depicted by point C′ in Fig. 1(c), vanish. Due to partial adiabaticity of the exit dynamics, C′ connects with A′ on the green circle, and the N mode leaves the cloud in such a way that its negative-refraction-like propagation is preserved. Therefore, adiabaticity plays a negative role at the entrance and a positive role at the exit.

Figure 4 shows propagation of the same Gaussian beam as in Fig. 3 for intermediate absorption, $\delta = 3\gamma$ and 7γ. By varying the detuning, one can control the P-mode exit intensity while keeping the N mode intact. For a large detuning and low absorption [Figs. 3(c) and 3(d)], nonadiabaticity of the exit with $L_* = 20\ \mu$m begins to play a role: The amplitude c_N grows both at the entrance and at the exit from the cloud. Counterintuitively, the N mode is generated in the regions of low, rather than high, gas density. Indeed, the transfer between the modes is due to their nonadiabatic coupling rather than reflection from the atomic planes.

VI. STABILIZATION OF THE N MODE

Figures 3(b) and 3(c) illustrate an important ingredient of our scheme. As the gas density increases, $\mathrm{Im}[k_P]$ increases as well, but $\mathrm{Im}[k_N]$ quickly reaches maximum and stabilizes. While for the parameters of Fig. 3 this behavior is barely seen, for higher gas densities and for k_z closer to π/a we observed formation of a well-defined maximum followed by strong suppression of $\mathrm{Im}[k_N]$ deeper in the gas cloud.

A similar phenomenon in another periodic system has been described in Ref. [24]: Considering the light eigenmodes in a purely absorptive cos-like grating as consisting of only the partial waves with the numbers 0 and -1, one finds that at strong potential strength one of the eigenmodes is stabilized. Similar stabilization is well known in quantum mechanics [25]. It is characterized by a branching point of the "exceptional point" type in the eigenvalues' dependence on the system parameters and is usually attributed to interference of the quantum amplitudes.

In a quantum-mechanical description, for a mode characterized by two amplitudes C_0 and C_{-1}, one would write the decay dynamics in the form

$$\dot{C}_0 = -i \int C_E V_{0,E}\, dE,$$
$$\dot{C}_{-1} = -i \int C_E V_{-1,E}\, dE, \qquad (20)$$
$$\dot{C}_E = -i V_{E,0} C_0 - i V_{E,-1},$$

where C_E are the bath mode amplitudes. If the coupling $V_{E,0} = V_{E,-1}$, then the asymmetric mode with $C_0 = -C_{-1}$ is stabilized ("destructive interference"), and the symmetric mode with $C_0 = C_{-1}$ undergoes fast decay ("constructive interference"). Light in an absorptive lattice can be described in an analogous way, with decay into bath modes due to Rayleigh scattering.

Unlike many quantum-mechanical phenomena, in our system the origin of the stabilization can be explicitly traced to the spatial symmetry properties of N and P modes. Indeed, Eq. (5) shows that near $k_z \simeq \pi/a$ the partial wave amplitudes P_m (of the P mode) and N_m (of the N mode) with $m = 0, -1$ are large, and all others are small. The relative signs of the amplitudes depend on whether the point on EFS, which corresponds to the m-th partial wave, is inside or outside the green dashed circle with the radius ω/c [see Fig. 1(c) and Eq. (5)]. For the N mode, point C representing the 0-th partial wave is inside, and point C′ representing the -1-st wave is outside the circle, therefore the signs of N_0 and N_{-1} differ. For the P mode, both 0-th and -1-st partial waves are represented by points outside the green circle, and the signs of P_0 and P_{-1} coincide. Therefore, the N mode is asymmetric, P mode is symmetric with respect to the atomic layer planes. This is seen in Fig. 3(e) showing the calculated distribution of field intensities.

We conclude that the N mode stabilizes because its field maxima are at the z values with no lattice atoms. The absence of absorption in the N mode allows us to choose small detunings from the resonance, thus weakening the requirement for the gas density.

VII. CONCLUSIONS AND OUTLOOK

In summary, this paper describes semiadiabatic dynamics of coupled optical modes (an optical analog of the quantum Landau-Zener dynamics), and explains stabilization of optical eigenmodes. It shows that their combination can solve the problem of negative refraction controlled in real time at a distance. We also specify a system where the experiment on negative refraction can be done with the present-day technology. Finally, we present a series of numerical calculations, finding the most important dependencies of these effects on the experimental parameters.

The proposed scheme realizes negative-refraction-like light propagation in a cold gas at the experimentally achieved density of 10^{13} cm^{-3}. This density estimate is three orders of magnitude lower than in the chirality-based proposals [7] and five orders of magnitude lower than in magnetic resonance-based proposals [6]. The advantage is due to the fact that our scheme does not rely on weak magnetic-dipole couplings employed in previous proposals. Stabilization of

the N mode against absorption further weakens the density requirements. Finally, due to the effect of the grating, a very weak contrast of ε (in our calculations, $\varepsilon_c \sim 10^{-2}$) is sufficient for strong modification of light propagation. At the same time, bandwidth of the negative refraction window is ∼20 times higher than the frequency window in EIT-based band-gap structures [12].

Our choice of the model atomic density profile allowed us to use concise equations for the field amplitudes C_m and to treat the mode dynamics analytically. This choice is substantiated by nowadays experimental techniques. A more smooth z distribution of atoms, such as, for example, $\varepsilon(z) = 1 + \varepsilon_c \cos ak$, would yield an infinite system of coupled equations for the amplitudes [14]. This would make the discussion less illustrative, while preserving the qualitative result: The negatively refracting mode is localized outside the maxima of atomic density. The more spread is the atomic distribution, however, the stronger is the undesired absorption of the N mode. A detailed study of these effects must be tied to the trapped gas temperature in a particular experiment: The higher the temperature, the more vibrational states of atoms in each lattice cite are excited and the stronger the atomic density spread in each lattice well.

Implementation of our scheme in higher-dimensional lattices with true negative refraction is straightforward. In conventional photonic crystals, high dielectric contrast is required to avoid the unwanted positively refracted wave [10]. In contrast, the present scheme can be employed even with small ε_c, since the birefrigence is suppressed via absorption of the P mode. Vaguely defined boundaries make the dynamics of light conceptually differ from that at a conventional interface. However, with reasonable length parameters one can transfer noticeable fraction of light into the N mode while fully controlling the intensity of the P mode at the exit. Nonadiabaticity is beneficial for the P- to N-mode energy transfer, and adiabaticity is good for preserving the N-mode character of the outgoing light. Intensity of the negatively refracted light will be higher for higher gas densities, smaller absorption, and angles closer to the Bragg angle.

ACKNOWLEDGMENTS

The authors are greatly indebted to discussions with Moshe Shapiro. His insight stimulated our work for many years. We are also pleased to thank M. Sukharev and K. W. Madison for consultations.

[1] *Physics of Negative Refraction and Negative Index Materials*, edited by C. M. Krowne and Y. Zhang (Springer, Berlin, 2007).

[2] J. B. Pendry, Physics **2**, 95 (2009); Y. Lai, J. Ng, H. Y. Chen, D. Z. Han, J. J. Xiao, Z.-Q. Zhang, and C. T. Chan, Phys. Rev. Lett. **102**, 253902 (2009).

[3] V. G. Veselago, Sov. Phys. Usp. **10**, 509 (1968); J. B. Pendry, Phys. Rev. Lett. **85**, 3966 (2000); P. V. Parimi, W. T. Lu, P. Vodo, and S. Sridhar, Nature **426**, 404 (2003).

[4] http://skullsinthestars.com/2009/05/19/what-does-negative-refraction-look-like/ and references therein; accessed on June (2014).

[5] H. Kosaka, T. Kawashima, A. Tomita, M. Notomi, T. Tamamura, T. Sato, and S. Kawakami, Phys. Rev. B **58**, R10096 (1998).

[6] M. Ö. Oktel and Ö. E. Müstecaplıoğlu, Phys. Rev. A **70**, 053806 (2004).

[7] J. Kästel, M. Fleischhauer, S. F. Yelin, and R. L. Walsworth, Phys. Rev. Lett. **99**, 073602 (2007); D. E. Sikes and D. D. Yavuz, Phys. Rev. A **82**, 011806(R) (2010).

[8] V. E. Kravtsov, V. M. Agranovich, and K. I. Grigorishin, Phys. Rev. B **44**, 4931 (1991).

[9] E. Cubukcu, K. Aydin, E. Ozbay, S. Foteinopoulou, C. M. Soukoulis, Nature **423**, 604 (2003); for a review, see S. Foteinopoulou, Physica B **407**, 4056 (2012) and references therein.

[10] M. Notomi, Phys. Rev. B **62**, 10696 (2000); S. Foteinopoulou and C. M. Soukoulis, *ibid.* **72**, 165112 (2005).

[11] G. Birkl, M. Gatzke, I. H. Deutsch, S. L. Rolston, and W. D. Phillips, Phys. Rev. Lett. **75**, 2823 (1995); I. H. Deutsch, R. J. C. Spreeuw, S. L. Rolston, and W. D. Phillips, Phys. Rev. A **52**, 1394 (1995); D. V. van Coevorden, R. Sprik, A. Tip, and A. Lagendijk, Phys. Rev. Lett. **77**, 2412 (1996); M. Antezza, Y. Castin, Phys. Rev. A **80**, 013816 (2009); S. Rist, C. Menotti, G. Morigi, *ibid.* **81**, 013404 (2010); A. Schilke, C. Zimmermann, P. W. Courteille, and W. Guerin, Phys. Rev. Lett. **106**, 223903 (2011); M. Samoylova, N. Piovella, R. Bachelard, and Ph.W. Courteille, Opt. Commun. **312**, 94 (2014).

[12] A. Andre and M. D. Lukin, Phys. Rev. Lett. **89**, 143602 (2002); D. Petrosyan, Phys. Rev. A **76**, 053823 (2007); M. Artoni and G. C. La Rocca, Phys. Rev. Lett. **96**, 073905 (2006); Y. Zhang *et al*, Op. Ex. **21**, 29338 (2013).

[13] C. Chin, A. J. Kerman, V. Vuletić, and S. Chu, Phys. Rev. Lett. **90**, 033201 (2003).

[14] P. St. J. Russel, Appl. Phys. B **39**, 231 (1986).

[15] F. B. Pedersen, G. T. Einevoll, and P. C. Hemmer, Phys. Rev. B **44**, 5470 (1991).

[16] R. S. Chu and T. Tamir, Proc. IEE **719**, 197 (1972); R.-S. Chu and J. A. Kong, IEEE Trans. Microwave Theor. Tech., **MTT-25**, 18 (1977).

[17] L. Allen and J. H. Eberly, *Optical Resonance and Two-Level Atoms* (Wiley-Interscience, New York, 1975).

[18] Daniel A. Steck, Cesium D Line Data, available online at http://steck.us/alkalidata (revision 2.0.1, 2 May 2008).

[19] We adopt bra" and "ket" notations of conventional quantum mechanics. Alternatively, one can use the formalism of biorthogonal states, see, e.g., N. Moiseyev, *Non-Hermitian Quantum Mechanics* (Cambrige University Press, Cambridge, 2011) and Refs. [20,21].

[20] M. V. Fedorov, M. A. Efremov, V. P. Yakovlev, and W. P. Schleich, J. Exp. Theor. Phys. **97**, 522 (2003).

[21] O. Atabek and R. Lefebvre, J. Phys. Chem. A **114**, 3031 (2010).

[22] M. S. Sarandy and D. A. Lidar, Phys. Rev. A **71**, 012331 (2005); A. Fleischer and N. Moiseyev, *ibid.* **72**, 032103 (2005); M. H. S. Amin, Phys. Rev. Lett. **102**, 220401 (2009).

[23] Q. Niu and M. G. Raizen, Phys. Rev. Lett. **80**, 3491 (1998).

[24] See M. V. Berry and D. H. J. O'Dell, J. Phys. A: Math. Gen. **31**, 2093 (1998); To compare with our case, one must assume complex σ in Eq. (8) and replace in Eq. (12) $\sigma/2$ with σ to account for $\delta(x)$-like instead of cos-like perturbation.

[25] The stabilization phenomenon is described in Ref. [24] in terms of the amplitudes of 0-th and -1-st partial waves coupled via the lattice. Compare, e.g., with strong-field interference stabilization in M. V. Fedorov, N. P. Poluektov, A. M. Popov *et al.*, IEEE J. Sel. Papers Quant. Electron. **18**, 42 (2012); formation of dark states via interference and EIT in M. Shapiro and P. Brumer, *Quantum Control of Molecular Processes* (Whiley-VCH, Weinheim, 2012) and M. Fleischhauer, A. Imamoglu, and J. P. Marangos, Rev. Mod. Phys. **77**, 633 (2005); as well as stabilization of atoms passing through an optical lattice in Ref. [20] and resonances of dissociating molecules in Ref. [21].